Article

Exploring the Structure and Properties of $V_wSe_yTe_{2-y}$ Mixed Crystals in the VTe2–VSe2 System

Sophia Kurig , Fabian Ketter , Anne Frommelius , B. Viliam Hakala , Jan van Leusen , Karen Friese , Richard Dronskowski *

Posted Date: 14 November 2023

doi: 10.20944/preprints202311.0867.v1

Keywords: ternary chalcogenide; X-ray diffraction; single-crystal; energy dispersive X-ray spectroscopy; magnetism; vanadium chalcogenide; VwSeyTe2–y

Article

Exploring the Structure and Properties of $V_wSe_yTe_{2-y}$ Mixed Crystals in the VTe_2–VSe_2 System

Sophia Kurig [1,†], Fabian Ketter [1,†], Anne Frommelius [1], B. Viliam Hakala [2], Jan van Leusen [1], Karen Friese [2] and Richard Dronskowski [1,3,*]

[1] Institute of Inorganic Chemistry, RWTH Aachen University, D-52056 Aachen, Germany
[2] Jülich Centre for Neutron Science-2 and Peter Grünberg Institute-4 (JCNS-2/PGI-4), Forschungszentrum Jülich GmbH, 52425 Jülich, Germany
[3] Hoffmann Institute of Advanced Materials, Shenzhen Polytechnic University, 7098 Liuxian Blvd, Nanshan District, Shenzhen 518055, China
* Correspondence: drons@HAL9000.ac.rwth-aachen.de; Tel.: +49-241-80-93642.
† These authors contributed equally to this work.

Dedicated to the memory of Professor Francis J. DiSalvo who passed away on October 27, 2023, aged 79.

Abstract: Vanadium(IV) chalcogenide materials are of increasing interest for use in catalysis and energy conversion-related applications. Since no ternary compounds are yet known in the V–Se–Te system, we studied ternary $V_wSe_yTe_{2-y}$ (w = 1.10, 1.13; y = 0.42, 0.72) phases crystallizing in space group $P\bar{3}m1$ (no. 164). Two single-crystal specimens with differing compositions of a solid solution were obtained using the ceramic method. All products were characterized by either single-crystal or powder X-ray diffraction. The lattice parameters increase with rising tellurium content in accordance to the larger ionic radius of the tellurium anion compared to selenium. The chemical compositions were confirmed by energy dispersive X-ray spectroscopy. Further, magnetic measurements revealed mostly antiferromagnetic properties. Simultaneous differential scanning calorimetry/thermogravimetric analyses in nitrogen atmosphere showed endothermic decomposition accompanied by the formation of VN. The results of this work can serve as a basis for the synthesis of new phases in the V–Se–Te and related vanadium chalcogenide systems.

Keywords: ternary chalcogenide; X-ray diffraction; single-crystal; energy dispersive X-ray spectroscopy; magnetism; vanadium chalcogenide; $V_wSe_yTe_{2-y}$

1. Introduction

Vanadium chalcogenides have remarkable properties in terms of magnetism and catalytic activity and are being used in important industrial processes. Exemplarily, the contact-process for the synthesis of sulfuric acid uses vanadium(V) oxide (V_2O_5) as a highly active catalyst in the oxidation step from SO_2 to SO_3 [1]. Vanadium selenides and tellurides exhibit promising electronic properties coupled to their structure and physical behavior. VSe_2 ($P\bar{3}m1$) shows good mechanical properties such as strength and durability together with electrical and optical qualities and is therefore applied in solar cells [2]. As anode material, VSe_2 is being tested for lithium- and sodium-ion batteries [3].

The bulk structures of vanadium chalcogenides were first explored in the middle of the 20th century [4-6]. Later, additional compounds belonging to these systems were found. This article elaborates on new members of the V–Se–Te system. The crystal structures of the previously reported materials VSe_2, $V_{1.04}Se_2$ and VTe_2 are shown in Figure 1.

Preprints (www.preprints.org) | NOT PEER-REVIEWED | Posted: 14 November 2023 doi:10.20944/preprints202311.0867.v1

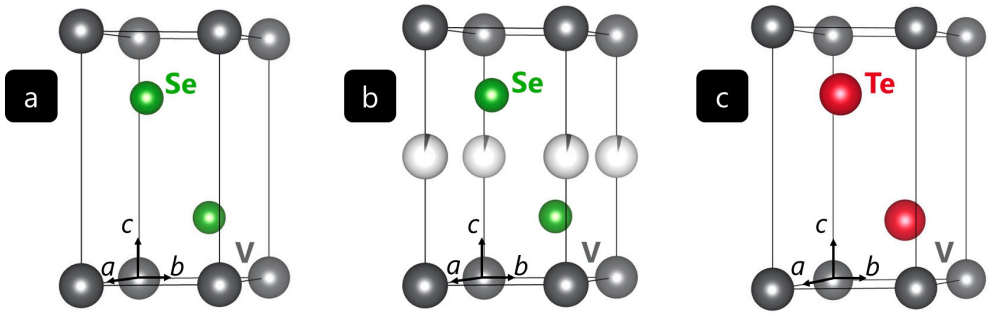

Figure 1. (a) Crystal structure of VSe_2 from powder XRD [7]. (b) Crystal structure of $V_{1.04}Se_2$ from single-crystal XRD [8]. (c) Crystal structure of VTe_2 from powder XRD [9]. Vanadium atoms in gray, selenium in green, tellurium in red.

As depicted in Figure 1, the crystal structures of the known vanadium(IV) selenides and tellurides adopt the trigonal space group $P\bar{3}m1$ ($Z = 1$). The structures (a) and (c) are representatives of the CdI_2-type in which vanadium atoms are located on Wyckoff site 1*a*. In structure (b), vanadium atoms additionally occupy Wyckoff site 1*b*, but only by 4%. The chalcogenide atoms are located on Wyckoff position 2*d* with $z = 0.257$ (a,b) and $z = 0.250$ (c) [7-9]. The crystal-chemical motif alludes to layers of vanadium cations that are octahedrally coordinated by the respective chalcogenide anions.

The different chalcogenide anions in the compounds VSe_2 and VTe_2 give rise to different properties, for example in terms of magnetism: VSe_2 is known as a paramagnetic compound and from a Curie-type contribution to its magnetic susceptibility originating from the vanadium atoms [10,11]. In contrast, VTe_2 evidences antiferromagnetic spin ordering below a Néel temperature of 418 °C. Furthermore, a transition of the polymorphic charge density wave at 753 °C can influence the magnetic behavior even at elevated temperatures [12,13].

The synthesis of new ternary vanadium dichalcogenides is not only auspicious because of versatile magnetic properties that could qualify mixed vanadium dichalcogenides for use in various applications. In contrast to the systems Cr–Se–Te [14-17] and Ti–Se–Te [5,18,19], where several ternary phases have been known since the middle of the 20th century, the system V–Se–Te is widely unexplored to date. Hence, we have decided to fill this gap, and we have synthesized a series of $V_wSe_yTe_{2-y}$ compounds supposedly belonging to a solid solution.

2. Results and Discussion

To validate both structure and composition, two single crystals and their structures were determined by X-ray diffraction. The stoichiometry found was then compared with energy dispersive X-ray spectroscopy data. The structural model was furthermore tested against Rietveld-derived results from powder data. According to Vegard's law, increasing lattice parameters were found with higher tellurium content. Also, the range of thermal decomposition was determined by simultaneous differential scanning calorimetry/thermogravimetric analysis. In addition, the magnetic behavior was studied.

2.1. Crystal structure description of $V_wSe_yTe_{2-y}$

The $V_wSe_yTe_{2-y}$ compounds were obtained as gray, crystalline powders from ceramic syntheses as described in 3.1. $V_{1.13}Se_{0.72}Te_{1.28}$ and $V_{1.10}Se_{0.42}Te_{1.58}$ crystallize with one structural formula per unit cell in the CdI_2-type belonging to the trigonal space group $P\bar{3}m1$ (no. 164) [7]. As alluded to already, CdI_2-type structures are known for their layered appearance consisting of layers of octahedrally coordinated metal ions. These layers are held together by van-der-Waals interactions. Figure 2 shows the unit cells as derived from single-crystal structure determination, as well as the layered structures.

Preprints (www.preprints.org) | NOT PEER-REVIEWED | Posted: 14 November 2023 doi:10.20944/preprints202311.0867.v1

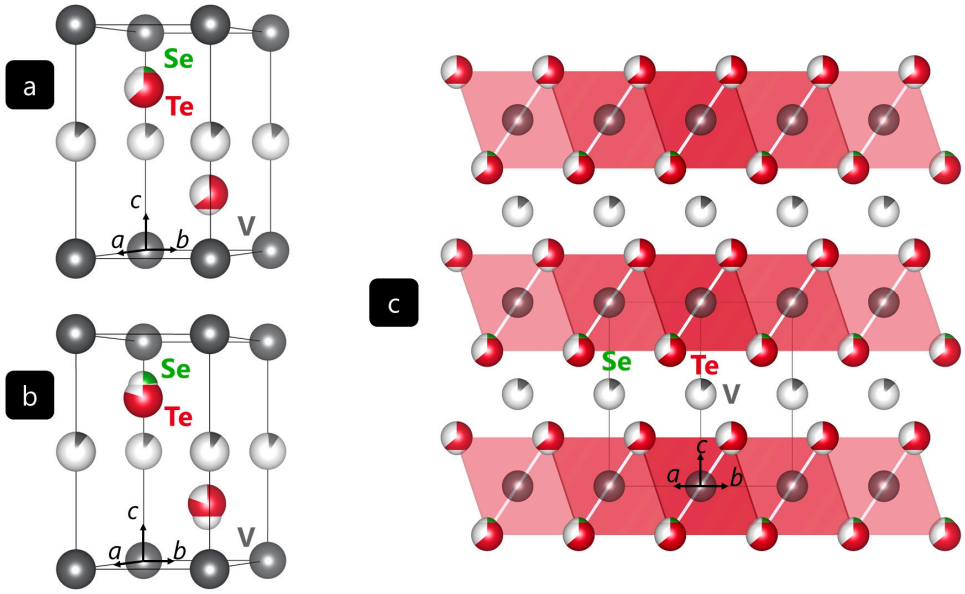

Figure 2. Crystal structure of (a) $V_{1.13}Se_{0.72}Te_{1.28}$ and (b) $V_{1.10}Se_{0.42}Te_{1.58}$ as derived from single-crystal XRD analysis; (c) layered structure of $V_{1.13}Se_{0.72}Te_{1.28}$.

In both structures, vanadium ions that are octahedrally coordinated by selenium or tellurium ions, respectively, reside on Wyckoff site 1*a* (V1, 0 0 0). Additionally, Wyckoff site 1*b* (V2, 0 ½ 0) is occupied with vanadium ions by 13% in the case of $V_{1.13}Se_{0.72}Te_{1.28}$ (a) and 10% in the case of $V_{1.10}Se_{0.42}Te_{1.58}$ (b), the Se atom found a little closer to the fully occupied layer formed by V1 than Te. In more detail, the selenium and tellurium ions coordinating the vanadium ions are located on Wyckoff site 2*d* (⅓ ⅔ *z*) with $z = 0.235(3)$ for selenium and $z = 0.265(1)$ for tellurium in $V_{1.13}Se_{0.72}Te_{1.28}$. In $V_{1.10}Se_{0.42}Te_{1.58}$, the selenium and tellurium *z* positions are 0.214(3) and 0.266(1), respectively. The results of the single-crystal refinements are summarized in Table 1, and the refined Wyckoff sites are given in Table S1.

It is worth mentioning that VS_4 is a promising material for magnesium ion batteries with an interchain spacing of 5.83 Å [20]. As the distances between the fully occupied vanadium layers are 6.29 Å and 6.36 Å for $V_{1.13}Se_{0.72}Te_{1.28}$ and $V_{1.10}Se_{0.42}Te_{1.58}$, respectively, it may well be the case that the aforementioned V-Se-Te phases may serve well in such magnesium ion batteries, since these distances appears to be large enough for Mg intercalation and deintercalation.

Table 1. Refinement details of the single-crystal studies of $V_{1.13}Se_{0.72}Te_{1.28}$ and $V_{1.10}Se_{0.42}Te_{1.58}$.

Formula	**$V_{1.13}Se_{0.72}Te_{1.28}$**	**$V_{1.10}Se_{0.42}Te_{1.58}$**
form wt. (g mol^{-1})	277.74	290.81
space group	$P\bar{3}m1$	$P\bar{3}m1$
a (Å)	3.626(2)	3.633(7)
c (Å)	6.290(2)	6.365(12)
volume (Å^3)	71.6(1)	72.7(3)
Z	1	1
calc. density (g cm^{-3})	6.441	6.639
μ (mm^{-1})	25.541	24.140
F(000)	117	122
θ range (°)	3.24–30.40	3.20–31.00
index range	$-5 \le h \le 4$ $-5 \le k \le 5$ $-8 \le l \le 8$	$-5 \le h \le 4$ $-4 \le k \le 5$ $-9 \le l \le 7$
reflections collected	1049	585
independent reflections	108	111

Preprints (www.preprints.org) | NOT PEER-REVIEWED | Posted: 14 November 2023 doi:10.20944/preprints202311.0867.v1

refinement method	Full matrix least squares on F^2	
data/restraints/parameters	108/0/11	111/0/14
goodness-of-fit on F^2	1.208	0.987
final R indices [$I > 2\sigma(I)$]	$R_1 = 0.021$; $wR_2 = 0.049$	$R1 = 0.020$; $wR_2 = 0.042$
R indices (all data)	$R_1 = 0.023$; $wR_2 = 0.050$	$R1 = 0.021$; $wR_2 = 0.042$
R_{int}	0.025	0.029
largest diff. peak and hole (e⁻Å⁻³)	1.454 and –1.198	0.807 and –0.904

2.2. Elemental analysis by means of energy dispersive X-ray diffraction

The elemental compositions were analyzed by energy dispersive X-ray spectroscopy (EDX) measurements of the isolated single crystals in a scanning electron microscope (SEM). The SEM images of both crystals are shown in Figure 3. The averaged elemental composition of the $V_{1.13}Se_{0.72}Te_{1.28}$ specimen analyzed from four single-crystal locations (white rectangles) was 30.7(4) at% vanadium, 27.0(4)% selenium, and 42.3(3)% tellurium. The vanadium content, according to the EDX data, is lower compared to findings from single-crystal XRD analysis. Seemingly, this is due to partial overlap of the vanadium $L_{\alpha 1}$ and $L_{\beta 1}$ signals with the oxygen $K_{\alpha 1}$ peak, which was found as a surface artefact [21]. The Se/Te ratio determined from the single-crystal XRD measurement is 0.56, close to the EDX value which arrives at 0.64. The EDX analysis thus confirms the composition of the newly synthesized phase, at least semi-quantitatively.

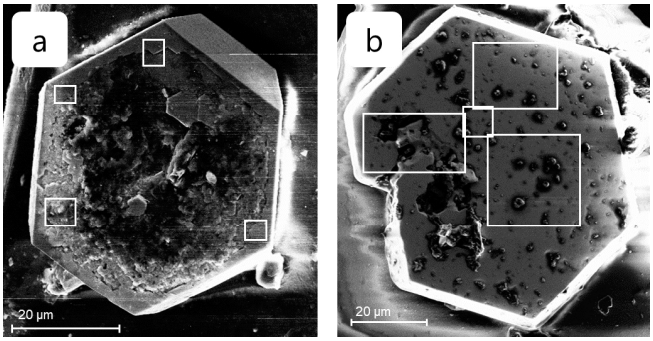

Figure 3. Scanning electron microscopy images of the isolated (a) $V_{1.13}Se_{0.72}Te_{1.28}$ and (b) $V_{1.10}Se_{0.42}Te_{1.58}$ single crystals. The white rectangles indicate where EDX measurements were performed.

For the crystal with the stoichiometry $V_{1.10}Se_{0.42}Te_{1.58}$, the EDX measurement also supports the finding of a lower selenium content. Again, the four-spot single-crystal composition was found as 34.7(2) at% vanadium, 9.4(3)% selenium, and 55.9(3)% tellurium. Clearly, the selenium content determined is lower compared to the single-crystal X-ray diffraction value, and we suspect the presence of tellurium-richer regions closer to the crystal surface. As EDX probes in a region of about 2 micrometers in depth, this might influence the result of this measurement [21]. Carbon artefacts were found in all EDX analyses. This contribution is a known effect for measurements on a carbon adhesive tape and was therefore neglected in data evaluation.

2.3. Powder X-Ray diffraction analysis of compounds in the V–Se–Te system.

Compounds with the refined compositions $VSe_{0.45}Te_{1.55}$, $VSe_{0.53}Te_{1.47}$, $VSe_{0.64}Te_{1.36}$, $VSe_{0.72}Te_{1.28}$, $VSe_{0.77}Te_{1.23}$, $VSe_{0.82}Te_{1.18}$, $VSe_{0.94}Te_{1.06}$ were synthesized as described in 3.1. All obtained products were gray and polycrystalline. Powder X-ray diffraction was carried out as described in 3.3, and the data were Rietveld-refined using the FullProf suite [22,23]. As a starting model, the solution of the single-crystal structure of $V_{1.13}Se_{0.72}Te_{1.28}$ was used. The chemical composition of tellurium and selenium was refined individually for each stoichiometry with the coefficient sum fixed to 2.

Interestingly, preferred orientation of the crystal to the (001) plane was observed, so the $G1$ parameter was refined to values between 0.27 and 0.40 indicating platy texture of the crystallites. This matches the shape of the hexagonal single-crystals and, reflecting the layered structure of the

Preprints (www.preprints.org) | NOT PEER-REVIEWED | Posted: 14 November 2023 doi:10.20944/preprints202311.0867.v1

material, is also known for related compounds such as VTe_2 [12]. Figure 4 shows the powder pattern of $VSe_{0.72}Te_{1.28}$ with the corresponding Rietveld refinement.

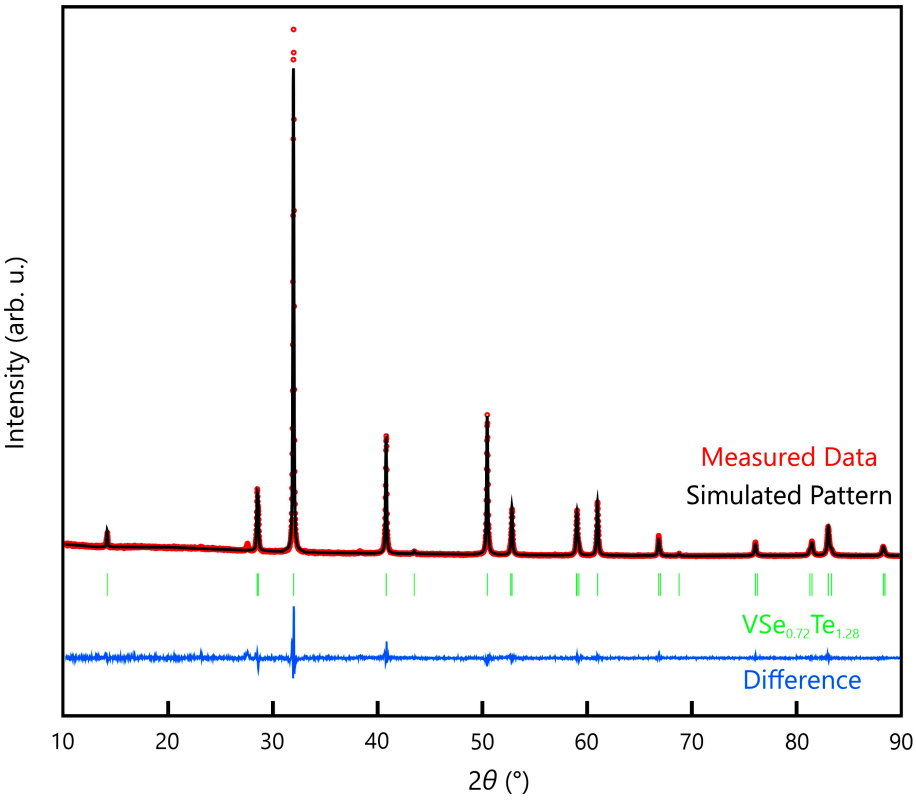

Figure 4. Rietveld refinement of the $VSe_{0.72}Te_{1.32}$ powder with measured data in red, simulated pattern in black, Bragg positions in green, and the difference between measured and calculated pattern in blue. One reflection of remaining tellurium at 27° was excluded in the refinement.

Figure 5 depicts powder-XRD patterns of VSe_yTe_{2-y} samples of different stoichiometries, with all reflections attributable to the respective Miller indices. With increasing tellurium content, we observe a shift towards lower 2θ values due to the lattice expansion satisfying the spatial requirement of the tellurium anion.

For describing the lattice parameters and the resulting unit-cell volume of similar mixed-ion compounds of the same space group, Vegard's law can be employed [24,25], relating the lattice parameters of mixed crystals to the lattice parameters of the corresponding pure solids weighted by the molar fraction of the respective constituent. For the ternary vanadium chalcogenides, Vegard's law is applicable upon comparing VSe_2 with 1*T*-VTe_2 [7,9]. Figure 6 shows the correlation of the unit cell volume with the tellurium content of the powder samples.

Preprints (www.preprints.org) | NOT PEER-REVIEWED | Posted: 14 November 2023 doi:10.20944/preprints202311.0867.v1

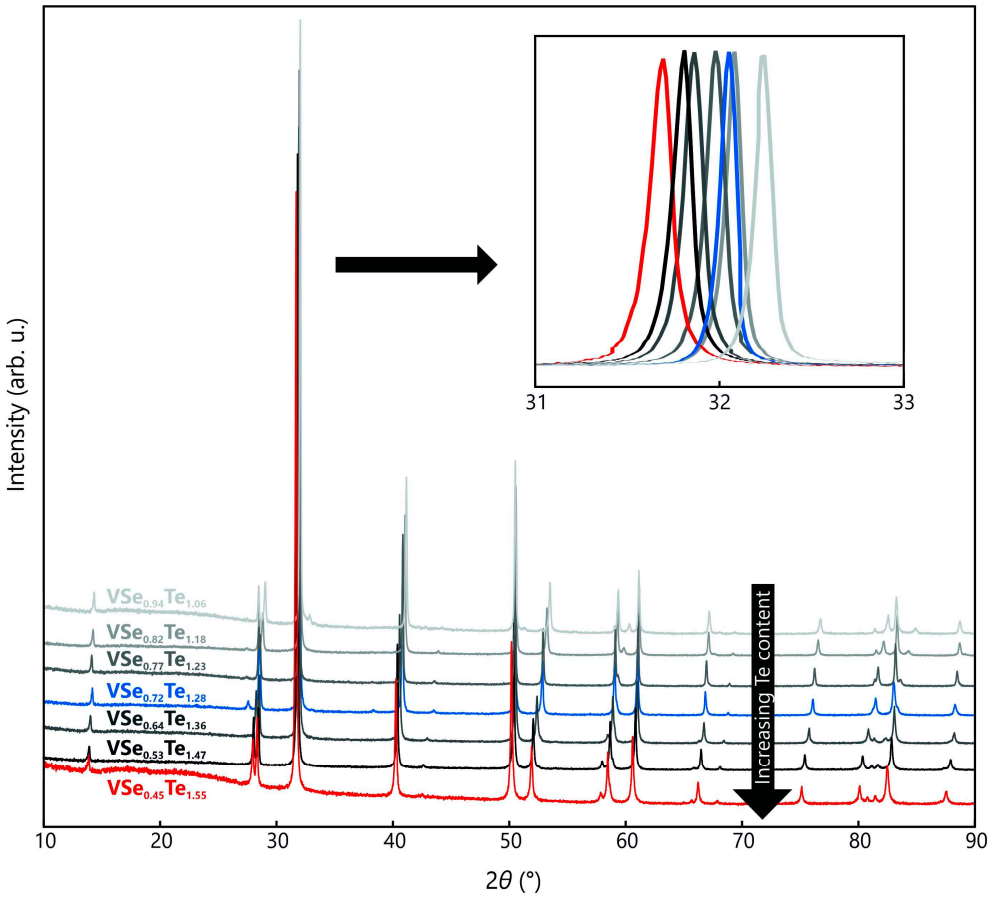

Figure 5. Powder XRD patterns of the VSe_yTe_{2-y} samples with different stoichiometries. Increasing tellurium content is marked in darker color tones. Samples from which single-crystals were isolated are shown in blue ($V_{1.13}Se_{0.72}Te_{1.28}$) and red ($V_{1.10}Se_{0.42}Te_{1.58}$).

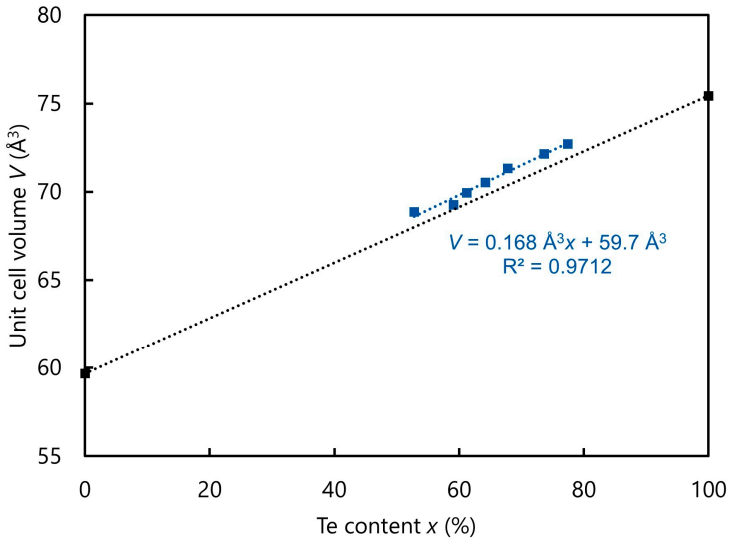

Figure 6. Unit cell volume of the synthesized ternary V–Se–Te compounds in space group $P\bar{3}m1$ depending on their tellurium content in blue and literature data for VSe_2 and VTe_2 in black [7,9].

As expected, the unit-cell volume increases with increasing tellurium content, explainable by the larger ionic radius of tellurium (2.21 Å for coordination number = 6) compared to selenium (1.98 Å for CN = 6) and thus an increase in spatial requirement [26]. The linear fit describes the experimental

Preprints (www.preprints.org) | NOT PEER-REVIEWED | Posted: 14 November 2023 doi:10.20944/preprints202311.0867.v1

volumes well, so Vegard's law applies to this system. Furthermore, the predicted unit cell volume of 59.7 Å^3 for pure VSe_2 corresponds to experimental findings by Wiegers (59.67 Å^3) [7].

Simultaneous DSC/TGA measurements in nitrogen atmosphere revealed an endothermic decomposition to VN at temperatures above approximately 850 °C. Mass loss and heat flow are shown in Figure S1 and the powder pattern in Figure S2. Initial investigations at low temperature show no obvious structural changes in $VSe_{0.72}Te_{1.28}$ down to 30K. The collected powder pattern is shown in Figure S3.

2.4. Magnetic measurements of $VSe_{0.72}Te_{1.28}$

The magnetic data of $VSe_{0.72}Te_{1.28}$ normalized to one formula unit are shown in Figure 7 as a $\chi_m T$ vs. T plot at 0.1 T and as a M_m vs. H plot at 2.0 K. At 300 K, $\chi_m T$ is 0.25 cm^3 K mol^{-1}, which is well below the range 0.34–0.38 cm^3 K mol^{-1} expected [27] from an isolated vanadium(IV) center. Upon cooling the compound, $\chi_m T$ almost linearly decreases to 0.083 cm^3 K mol^{-1} at 17 K, and subsequently drops to 0.054 cm^3 K mol^{-1} at 2.8 K. At 2.0 K, the molar magnetization continuously increases by increasing the applied magnetic field. At 50 kOe, the M_m vs. H curve is characterized by a distinct slope and the value $M_m = 0.09\ N_A\ \mu_B$. Both observations show that the magnetization is far from being saturated under these conditions. E.g., the saturation value is $M_{m,sat} = gS\ N_A\ \mu_B \approx 1.0\ N_A\ \mu_B$ for a vanadium(IV) center with the valence electron configuration $3d^1$, an effective g value of $g \approx 2.0$ and spin $S = ½$.

Even though a slight deviation from the spin-only value of $\chi_m T = 0.375$ cm^3 K mol^{-1} ($S = ½$) is expected for a $3d^1$ center even in a perfect octahedral ligand field, since contributions from the orbital momentum are not fully quenched, the found value at 300 K is beyond such an explanation. However, the value of 0.25 cm^3 K mol^{-1} as well as the distinct slope of the $\chi_m T$ vs. T curve over the entire measured temperature range (instead of being almost constant) indicate predominantly strong antiferromagnetic exchange interactions between the vanadium centers. This conclusion is also supported by the magnetization data at 2.0 K, since strong antiferromagnetic interactions result in the observed and above discussed features of the M_m vs. H curve.

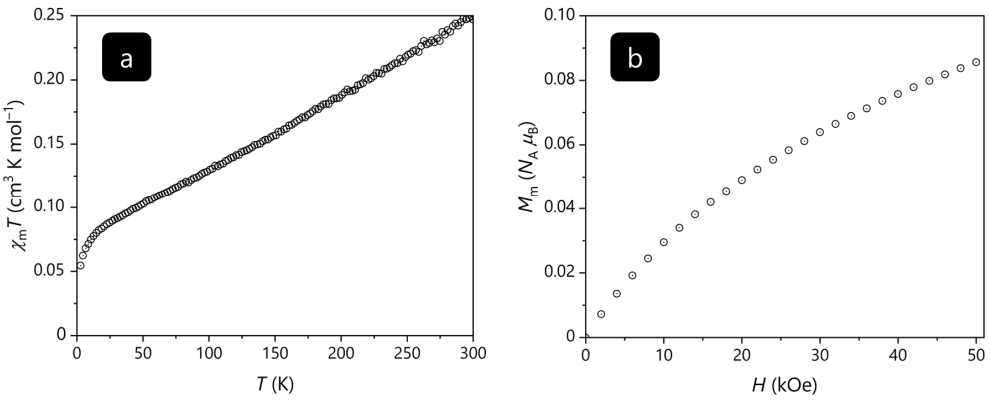

Figure 7. (a) Temperature dependence of $\chi_m T$ of $VSe_{0.72}Te_{1.28}$ at 0.1 T, (b) molar magnetization M_m vs. applied magnetic field H at 2.0 K.

3. Materials and Methods

3.1. Syntheses

Ceramic syntheses were carried out starting from pure vanadium (99.5%, Alfa Aesar), selenium (99.999%, MaTeck), and tellurium (≥ 99.7%, Fluka AG) in stoichiometric quantities (≈ 300 mg per experiment) in evacuated quartz glass ampoules (length 9 cm, diameter 0.7 cm) in a horizontal tube furnace. The applied temperature program involved heating to 800 °C with a rate of 80 °C h^{-1}, holding this temperature for 120 h, and subsequently quenching in icy water for all phases. The reaction products were gray, metallically lustering powders containing small crystals that were isolated and

analyzed with single-crystal X-ray diffraction experiments. So far, the powders appear as being stable in air for at least one year.

3.2. Single-crystal X-Ray diffraction experiments and structure resolution

Single-crystal X-ray diffraction experiments were carried out on a Bruker APEX II diffractometer (Bruker Corporation, Billerica, MA, USA) with Mo-K_α (λ = 0.71073 Å) radiation using a CCD detector. Integration and absorption correction of the experimental data was carried out with APEX2 [28]. The structures were solved and refined using direct methods in WinGX 2023.1 [29] and SHELXL 2018/1 [30-32]. The well-resolved data allowed to refine the fully occupied V1 (1*a*) and sub-occupied V2 (1*b*) positions with independent anisotropic displacement parameters (ADPs). Because the Se and Te essentially occupy the same (2*b*) site, with only a small displacement difference of about 0.33 Å ($V_{1.10}Se_{0.42}Te_{1.58}$) and 0.19 Å ($V_{1.13}Se_{0.72}Te_{1.28}$), their site-occupation factors were coupled to full occupancy for the 2*b* site. The larger displacement difference in $V_{1.10}Se_{0.42}Te_{1.58}$ allowed to refine Se and Te with individual ADPs while in $V_{1.13}Se_{0.72}Te_{1.28}$ a common ADP set for Se and Te atoms was used. Full details concerning the structure determinations are available in CIF format and have been deposited as CCDC 2306778 and 2306779. These data can be obtained free of charge via www.ccdc.cam.ac.uk/data_request/cif, or by emailing data_request@ccdc.cam.ac.uk, or by contacting The Cambridge Crystallographic Data Centre, 12 Union Road, Cambridge CB2 1EZ, UK; fax: +44 1223 336033.

3.3. Powder X-Ray diffraction experiments and refinement

To obtain powder X-ray diffraction data, the gray reaction products were mechanically ground and placed between Mylar sheets in a sample holder. Powder X-ray diffraction analysis was carried out on a STADI P powder diffractometer (STOE & CIE GmbH, Darmstadt, Germany) equipped with a DECTRIS® MYTHEN detector and Ge single-crystal monochromator with Cu-$K_{\alpha1}$ radiation (λ = 1.54059 Å). Powder X-Ray diffraction measurements were controlled with the aid of the WinXPow software [33].

Data refinement was carried out using the Rietveld method with the FullProf suite [22], starting with a model derived from the single-crystal structure refinement of $V_{1.13}Se_{0.72}Te_{1.28}$.

Low temperature data were collected on a Huber G670 powder diffractometer (HUBER Diffraktionstechnik GmbH & Co. KG, Rimsting, Germany) equipped with a copper X-ray tube in combination with a Ge Huber 616.2 monochromator.

3.4. Scanning Electron Microscopy (SEM) with Energy dispersive X-ray spectroscopy measurements (EDX)

Energy dispersive X-ray spectroscopy measurements (EDX) were carried out on a Leo Supra 35 VP scanning electron microscope (SEM) from Carl Zeiss AG (Oberkochen, Germany). By means of an acceleration voltages of 10 kV, the measurements were performed using an INCA Energy 200 spectroscope with a SiLi crystal (133 eV, 10 mm^2) from Oxford Instruments (Abingdon, UK). For the measurement, the sample was deposited on a carbon sticky tape pasted on an aluminium holder.

3.5. Measurements of the magnetic properties

A Quantum Design DynaCool physical property measurement system (PPMS) (Quantum Design International, Inc., San Diego, CA, USA) was used in the vibrating sample magnetometry (VSM) option. A polycrystalline sample of $VSe_{0.77}Te_{1.23}$ was immobilized using a polypropylene sample capsule and a brass holder. The data were measured as a function of temperature (2–300 K at 0.1 T) and magnetic field (0.1–5 T at 2 K), then corrected for the diamagnetic contributions of the sample holder and the compound ($\chi_{m,dia} = -1.37\times10^{-4}$ cm^3 mol^{-1}).

4. Conclusions

The new ternary compounds exhibit similar structures to the already known $V_{1.04}Se_2$ phase and a high-temperature modification of VTe_2 [8,9]. The selenium and tellurium atoms, respectively,

occupy the Wyckoff site 2*d*, and the lattice parameters were found to lie between the ones of the structures of the binaries. Powder diffractograms of seven compounds of different stoichiometries within the $V_wSe_yTe_{2-y}$ system evidence the expected trend, namely that a larger tellurium content leads to a shift of the reflection positions to lower 2 values.

Simultaneous DSC/TGA measurements in nitrogen atmosphere revealed an endothermic decomposition to VN at temperatures above approximately 850 °C. The magnetic measurements evidences predominantly strong antiferromagnetic coupling.

Supplementary Materials: Single-crystal data in CIF format can be downloaded at: Preprints.org, Table S1: Spatial parameters in $V_{1.13}Se_{0.72}Te_{1.28}$ and $V_{1.10}Se_{0.42}Te_{1.58}$; Figure S1: Thermogravimetric analysis and differential scanning calorimetry of $VSe_{0.72}Te_{1.28}$; Figure S2: Comparison of $VSe_{0.72}Te_{1.28}$ powder X-ray data after synthesis, after DSC/TGA, and Bragg positions of VSe and VN; Figure S3: Comparison of $VSe_{0.72}Te_{1.28}$ powder X-ray data at room temperature and at 30 K.

Author Contributions: Conceptualization S.K.; methodology S.K., A.F., B.V.H. and J.v.L.; validation J.v.L. and R.D.; formal analysis F.K., S.K., A.F. and J.v.L.; investigation F.K., S.K., A.F. and B.V.H.; resources B.V.H., A.F., K.F. and R.D.; data curation S.K.; writing—original draft preparation F.K. and S.K.; writing—review and editing S.K., F.K., A.F., B.V.H., J.v.L., K.F. and R.D.; visualization F.K., S.K. and J.v.L.; supervision K.F. and R.D.; project administration, S.K., K.F. and R.D.; funding acquisition K.F. and R.D. All authors have read and agreed to the published version of the manuscript.

Funding: This research was funded by the German Research Foundation (DFG, Bonn, Germany; SFB 917 "Nanoswitches"; S.K., B.V.H., K.F. and R.D.).

Data Availability Statement: The crystallographic data of $V_{1.10}Se_{0.42}Te_{1.58}$ and $V_{1.13}Se_{0.72}Te_{1.28}$ are provided in separate CIF files.

Acknowledgments: The authors thank Tobias Storp for the collection of powder and single-crystal X-ray diffraction data, Birgit Hahn for EDX measurements and Dr. Shibabrata Nandi and Hend Shahed for their assistance with the PPMS measurement.

Conflicts of Interest: The authors declare no conflict of interest.

References

1. Dunn, J.P.; Stenger, H.G.; Wachs, I.E. Oxidation of SO_2 over Supported Metal Oxide Catalysts. *J. Catal.* **1999**, *181*, 233-243, doi:https://doi.org/10.1006/jcat.1998.2305.
2. Sanap, P.P.; Gupta, S.P.; Kahandal, S.S.; Gunjakar, J.L.; Lokhande, C.D.; Sankapal, B.R.; Said, Z.; Bulakhe, R.N.; Man Kim, J.; Bhalerao, A.B. Exploring vanadium-chalcogenides toward solar cell application: A review. *J. Ind. Eng. Chem.* **2023**, doi:https://doi.org/10.1016/j.jiec.2023.09.004.
3. Yang, X.; Zhang, Z. Carbon-coated vanadium selenide as anode for lithium-ion batteries and sodium-ion batteries with enhanced electrochemical performance. *Mater. Lett.* **2017**, *189*, 152-155, doi:https://doi.org/10.1016/j.matlet.2016.12.001.
4. Hoschek, E.; Klemm, W. Vanadinselenide. *Z. Anorg. Allg. Chem.* **1939**, *242*, 49-62, doi:https://doi.org/10.1002/zaac.19392420106.
5. Ehrlich, P. Über die binären Systeme des Titans mit den Elementen Stickstoff, Kohlenstoff, Bor und Beryllium. *Z. Anorg. Chem.* **1949**, *259*, 1-41, doi:https://doi.org/10.1002/zaac.19492590102.
6. Biltz, W.; Köcher, A. Beiträge zur systematischen Verwandtschaftslehre. 88. Über das System Vanadium/Schwefel. *Z. Anorg. Allg. Chem.* **1939**, *241*, 324-337, doi:https://doi.org/10.1002/zaac.19392410402.
7. Wiegers, G.A. Physical properties of first-row transition metal dichalcogenides and their intercalates. *Physica B+C* **1980**, *99*, 151-165, doi:https://doi.org/10.1016/0378-4363(80)90225-9.
8. Nakahira, M.; Hayashi, K. Characterization of the layered transition-metal dichalcogenides with octahedral coordination. *Mat. Res. Bull.* **1978**, *13*, 1403-1408, doi:https://doi.org/10.1016/0025-5408(78)90132-0.
9. Bronsema, K.D.; Bus, G.W.; Wiegers, G.A. The crystal structure of vanadium ditelluride, $V_{1+x}Te_2$. *J. Solid State Chem.* **1984**, *53*, 415-421, doi:https://doi.org/10.1016/0022-4596(84)90120-8.
10. van Bruggen, C.F.; Haas, C. Magnetic susceptibility and electrical properties of VSe_2 single crystals. *Solid State Commun.* **1976**, *20*, 251-254, doi:https://doi.org/10.1016/0038-1098(76)90187-3.
11. DiSalvo, F.J.; Waszczak, J.V. Magnetic studies of VSe_2. *Phys. Rev. B* **1981**, *23*, 457-461, doi:https://doi.org/10.1103/PhysRevB.23.457.
12. Won, D.; Kiem, D.H.; Cho, H.; Kim, D.; Kim, Y.; Jeong, M.Y.; Seo, C.; Kim, J.; Park, J.-G.; Han, M.J.; et al. Polymorphic Spin, Charge, and Lattice Waves in Vanadium Ditelluride. *Adv. Mat.* **2020**, *32*, 1906578, doi:https://doi.org/10.1002/adma.201906578.

13. Duvjir, G.; Jung, J.-A.; Ly, T.T.; Lam, N.H.; Chang, Y.J.; Lee, S.; Kim, H.; Kim, J. Fine structure of the charge density wave in bulk VTe_2. *APL Mater.* **2022**, *10*, doi:https://doi.org/10.1063/5.0117992
14. Huang, Z.-L.; Bensch, W.; Benea, D.; Ebert, H. Anion substitution effects on structure and magnetism in the chromium chalcogenide Cr_5Te_8—Part I: Cluster glass behavior in trigonal $Cr_{(1+x)}Q_2$ with basic cell (Q=Te, Se; Te:Se=7:1). *J. Solid State Chem.* **2004**, *177*, 3245-3253, doi:https://doi.org/10.1016/j.jssc.2004.05.046.
15. Lotgering, F.K.; Gorter, E.W. Solid solutions between ferromagnetic and antiferromagnetic compounds with NiAs structure. *J. Phys. Chem. Solids* **1957**, *3*, 238-249, doi:https://doi.org/10.1016/0022-3697(57)90028-8.
16. Tsubokawa, I. The Magnetic Properties of Chromium-Tellurium-Selenium System. *J. Phys. Soc. Jpn.* **1956**, *11*, 662-665, doi:https://doi.org/10.1143/JPSJ.11.662.
17. Wontcheu, J.; Bensch, W.; Mankovsky, S.; Polesya, S.; Ebert, H.; Kremer, R.K.; Brücher, E. Anion substitution effects on the structure and magnetism of the chromium chalcogenide Cr_5Te_8—Part III: Structures and magnetism of the high-temperature modification $Cr_{(1+x)}Q_2$ and the low-temperature modification $Cr_{(5+x)}Q_8$ (Q=Te, Se; Te:Se=5:3). *J. Solid State Chem.* **2008**, *181*, 1492-1505, doi:https://doi.org/10.1016/j.jssc.2008.03.021.
18. Arnaud, Y.; Chevreton, M. Etude comparative des composés TiX_2 (X = S, Se, Te). Structures de $TiTe_2$ et TiSeTe. *J. Solid State Chem.* **1981**, *39*, 230-239, doi:https://doi.org/10.1016/0022-4596(81)90336-4.
19. Rimmington, H.P.B.; Balchin, A.A. The growth by iodine vapour transport techniques and the crystal structures of layer compounds in the series TiS_xSe_{2-x}, TiS_xTe_{2-x}, $TiSe_xTe_{2-x}$. *J. Crystal Growth* **1974**, *21*, 171-181, doi:https://doi.org/10.1016/0022-0248(74)90001-3.
20. Dey, S.; Lee, J.; Britto, S.; Stratford, J.M.; Keyzer, E.N.; Dunstan, M.T.; Cibin, G.; Cassidy, S.J.; Elgaml, M.; Grey, C.P. Exploring Cation–Anion Redox Processes in One-Dimensional Linear Chain Vanadium Tetrasulfide Rechargeable Magnesium Ion Cathodes. *J. Am. Chem. Soc.* **2020**, *142*, 19588-19601, doi:https://doi.org/10.1021/jacs.0c08222.
21. Goldstein, J.I.; Newbury, D.E.; Michael, J.R.; Ritchie, N.W.M.; Scott, J.H.J.; Joy, D.C. *Scanning Electron Microscopy and X-Ray Microanalysis*, 4 ed.; Springer New York, NY: New York, NY, USA, 2017.
22. Rodríguez-Carvajal, J. Recent advances in magnetic structure determination by neutron powder diffraction. *Phys. B: Condens. Matter.* **1993**, *192*, 55-69, doi:https://doi.org/10.1016/0921-4526(93)90108-I.
23. Rodríguez-Carvajal, J. Recent developments of the program FULLPROF. *Commission on Powder Diffraction (IUCr) Newsletter* **2001**, *26*, 12.
24. Vegard, L. Die Konstitution der Mischkristalle und die Raumfüllung der Atome. *Z. Phys.* **1921**, *5*, 17-26, doi:https://doi.org/10.1007/BF01349680.
25. Goldschmidt, V.M. Die Gesetze der Krystallochemie. *Naturwissenschaften* **1926**, *14*, 477-485, doi:https://doi.org/10.1007/BF01507527.
26. Shannon, R. Revised effective ionic radii and systematic studies of interatomic distances in halides and chalcogenides. *Acta Crystallogr. A* **1976**, *32*, 751-767, doi:https://doi.org/10.1107/S0567739476001551.
27. Lueken, H. *Magnetochemie*; Teubner Verlag: Stuttgart, Germany, 1999.
28. *APEX2*, v2014.11-0; Bruker AXS: Madison, WI, USA, 2015.
29. Farrugia, L. WinGX and ORTEP for Windows: an update. *J. Appl. Cryst.* **2012**, *45*, 849-854, doi:https://doi.org/10.1107/S0021889812029111.
30. Sheldrick, G. A short history of SHELX. *Acta Crystallogr. A* **2008**, *64*, 112-122, doi:https://doi.org/10.1107/S0108767307043930.
31. Sheldrick, G. Crystal structure refinement with SHELXL. *Acta Crystallogr. C* **2015**, *71*, 3-8, doi:https://doi.org/10.1107/S2053229614024218.
32. Sheldrick, G. SHELXT - Integrated space-group and crystal-structure determination. *Acta Crystallogr. A* **2015**, *71*, 3-8, doi:https://doi.org/10.1107/S2053273314026370.
33. *WinXPOW Powder Diffraction Software*, 3.7.0.0; STOE & Cie GmbH: Hilpertstr. 10, 64295 Darmstadt, Germany, 2021.
34. Sakuma, T.; Xianglian; Siagian, S.; Basar, K.; Takahashi, H.; Igawa, N.; Kamishima, O. Correlation effects among thermal displacements of atoms in VSe by diffuse neutron scattering measurement. *J. Therm. Anal. Calorim.* **2010**, *99*, 173-176, doi:https://doi.org/10.1007/s10973-009-0501-x.
35. Sharygin, V.V.; Ripp, G.S.; Yakovlev, G.A.; Seryotkin, Y.V.; Karmanov, N.S.; Izbrodin, I.A.; Grokhovsky, V.I.; Khromova, E.A. Uakitite, VN, a New Mononitride Mineral from Uakit Iron Meteorite (IIAB). *Minerals* **2020**, *10*, 150, doi:https://doi.org/10.3390/min10020150.
36. Lengauer, W.; Ettmayer, P. Lattice parameters and thermal expansion of δ-VN_{1-x} from 298–1000 K. *Monatsh. Chem.* **1986**, *117*, 713-719, doi:https://doi.org/10.1007/BF00810062.
37. Ettmayer, P.; Schebesta, W.; Vendl, A.; Kieffer, R. Beitrag zur Kenntnis des Systems Vanadin—Chrom—Stickstoff. *Monatsh. Chem.* **1978**, *109*, 929-941, doi:https://doi.org/10.1007/BF00907315.

 doi:10.20944/preprints202311.0867.v1

disclaim responsibility for any injury to people or property resulting from any ideas, methods, instructions or products referred to in the content.